Supplementary Information

Nitrogen-inserted nickel nanosheets with controlled orbital hybridization and strain fields for boosted hydrogen oxidation in alkaline electrolytes

Xu Zhao,[†,a] Xiangyang Li,[†,b] Lulu An,[a] Kevin Iputera,[c] Jiang Zhu,[a] Pengfei Gao,[b] Ru-Shi Liu,*[c] Zhenmeng Peng,*[d] Jinlong Yang*[b] and Deli Wang*[a]

[a]Key laboratory of Material Chemistry for Energy Conversion and Storage (Ministry of Education), Hubei Key Laboratory of Material Chemistry and Service Failure, School of Chemistry and Chemical Engineering, Huazhong University of Science and Technology, Wuhan, Hubei, 430074, P. R. China.

[b]Hefei National Laboratory for Physical Sciences at the Microscale, Synergetic Innovation Center of Quantum Information and Quantum Physics, University of Science and Technology of China, Hefei, Anhui, 230026, P. R. China.

[c]Department of Chemistry, National Taiwan University, Taipei 106, Taiwan.

[d]Department of Chemical and Biomolecular Engineering, University of Akron, Akron, Ohio 44325, United States.

[†]These authors contributed equally to this work.

**Corresponding authors*: rsliu@ntu.edu.tw (R. S. Liu), zpeng@uakron.edu (Z. M. Peng) jlyang@ustc.edu.cn (J. L. Yang), wangdl81125@hust.edu.cn (D. L. Wang)

Experimental sections

Chemicals and materials.

Nickel (III) nitrate hexahydrate ($Ni(NO)_3 \cdot 6H_2O$), 1-Methyl-2-pyrrolidone (C_5H_9NO), ethanol (C_2H_6O), isopropyl alcohol (C_3H_8O), and potassium hydroxide (KOH) were purchased from Sinopharm Chemical Reagent Co. Ltd (Shanghai, China). Ultrapure water with a resistivity of 18.2 MΩ cm was used in all experiments.

Materials synthesis.

In a typical synthesis, the N-Ni nanosheets were prepared by a two-step method. First, sheet-like $Ni(OH)_2$ precursors were synthesized by using a solvothermal route with modification.[1] Briefly, $Ni(NO)_3 \cdot 6H_2O$ (3 mmol) was dissolved in a mixture of C_5H_9NO (27 mL) and DI water (3 mL) via magnetic stirring for 30 min, which was then transferred into a Teflon-lined autoclave and kept reacting at 180 ^oC for 6 h. After cooling to room temperature, $Ni(OH)_2$ precursors were collected and dried under vacuum. For the synthesis of N-Ni nanosheets, 30 mg of the $Ni(OH)_2$ precursors were placed in the quartz tube and heated at 350 °C for 4h under NH_3 atmosphere with a flow rate of 100 sccm. After that, the final 4.3%N-Ni nanosheets were obtained. Furthermore, 3.5%N-Ni nanosheets and 1.6% N-Ni nanosheets could also be prepared via similar reduction procedures, except using the reducing atmosphere of NH_3/Ar (80/20 sccm) and NH_3/Ar (60/40 sccm), respectively. In addition, pure Ni nanosheets could be obtained by heating the precursors at 400 °C for 4h in the reducing atmosphere of H_2/Ar (10/90 sccm).

X-ray absorption spectroscopy measurements.

XAS spectra were collected from the 17C1 beamline of the National Synchrotron Radiation Research Center (NSRRC) in Hsinchu, Taiwan. The storage work at 1.50 GeV with a beam current of 360 mA. The fluorescence mode was used to characterize all XAS results. The X-ray pre-edge and post-edge absorption were normalized to 0 and 1, respectively.

DFT calculations.

Density functional theory calculations were performed to investigate the hydrogen oxidation reaction on the N-Ni and pure Ni structures within the Perdew-Burke-Ernzerholf (PBE) generalized gradient approximation (GGA), which is implemented in Vienna ab initio Simulation Package (VASP).[2] The projected augmented wave (PAW) method was used by the plane-wave basis with a kinetic cutoff energy of 500 eV.[3] To avoid periodic image interactions, a vacuum layer of about 15 Å was adopted along the z-axis for all the slab models. The Ni(111) surface with four Ni layers containing 64 atoms was simulated. The Brillouin zone was sampled by a 2×3×1 k-points grid. All atoms except those in the bottom two Ni layers were fully relaxed until the residual force was less than 0.01 eV/Å. The convergence criterion for the total energy was set to 1×10^{-6} eV. DFT-D2 method proposed by Grimme was adopted for van der Waals interactions.[4] Similar method was also performed for the N-Ni(111) surface, in which the N atoms tended to be in the body-center site of the bulk Ni structure. To simulate the N-Ni(111) surface with Ni-Ni coordination missing, we randomly dug out an exposed Ni atom on the surface layer.

The HBE values were calculated by using the following equation:

$$\mathrm{HBE} = E_{\mathrm{H@cat.}} - E_{\mathrm{cat.}} - E_{\mathrm{H}} \quad (1)$$

The OHBE values were calculated by using the following equation:

$$\mathrm{OHBE} = E_{\mathrm{OH@cat.}} - E_{\mathrm{cat.}} - E_{\mathrm{OH}} \quad (2)$$

where $E_{\mathrm{H@cat.}}$ and $E_{\mathrm{OH@cat.}}$ are the total energies of catalyst surface with adsorbed H and OH species, respectively; $E_{\mathrm{cat.}}$ represents the energies of catalyst surface; E_{H} is one-half the energy of gas-phase H_2; E_{OH} represents the energy of gas-phase H_2O minus one-half the energy of gas-phase H_2.

The hydrogen adsorption free energy was determined as $\Delta G = \mathrm{HBE} + \Delta E_{\mathrm{ZPE}} - T\Delta S$, where ΔE_{ZPE} and ΔS are zero-point energy correction and entropy change of hydrogen adsorption, respectively. At T=298.15 K, ΔG can be calculated by ΔG = HBE + 0.24 eV.[5]

Electrochemical measurements.

All the HOR electrochemical measurements were performed at a CHI660E electrochemical workstation at room temperature. A graphite rod and a reversible hydrogen electrode were employed as the counter and reference electrode, respectively. To prepare the working

electrode, 5 mg of N-Ni catalysts with Vulcan XC-72 carbon supports were dispersed in a mixture containing 1 mL of isopropyl alcohol and 15 μL of 5 wt% Nafion solution under ultrasonication for 1 h. A certain amount of the suspension was deposited on the RDE with the loading amount to be 0.32 mg cm^{-2}. Before HOR measurements, the 0.1 M KOH electrolytes were purged with high-purity H_2 for half an hour. The polarization curves were measured at a rotating speed of 1600 rpm with a scan rate of 1 mV s^{-1}. All the polarization curves were *iR*-corrected. The accelerated durability tests were performed by potential cycling in the range of -0.05-0.15 V for 2000 cycles with a scan rate of 100 mV s^{-1} in H_2-saturated 0.1 M KOH electrolyte. After that, a polarization curve at a scan rate of 1 mV s^{-1} was recorded. The chronoamperometry tests were carried out at a constant potential of 50 mV in H_2-saturated 0.1 M KOH electrolyte. Electrochemical active surface areas (ECSAs) were obtained by conducting cyclic voltammetry at the potential region from -0.15-0.6 V in N_2-saturated 0.1 M KOH electrolyte with a scan rate of 50 mV s^{-1}. The value of ECSA was calculated from the integrated region of OH desorption at the backward scan. The mass activities were obtained by normalizing the kinetic current to the loading mass of catalysts. The specific activities were elevated through normalizing the exchange current to the real active surface area of catalysts.

The kinetic current density (j_k) was calculated by the Koutecky-Levich equation:

$$\frac{1}{j} = \frac{1}{j_k} + \frac{1}{j_d} = \frac{1}{j_k} + \frac{1}{Bc_0\omega^{1/2}} \quad (3)$$

where j, j_d, B, c_0 and ω are the measured current density, diffusion-limited current, the Levich constant, the solubility of H_2 in alkaline solution and the rotation speed of the electrode, respectively.

The exchange current density (j_0) could be calculated from the Butler-Volmer equation:

$$j_k = j_0\left(e^{\frac{\alpha F}{RT}\eta} - e^{\frac{(1-\alpha)F}{RT}\eta}\right) \quad (4)$$

where α, η and T refer to the charge transfer coefficient, overpotential and the operating temperature, respectively. F and R correspond to the Faraday constant and the universal gas constant, respectively.

Characterization techniques.

TEM images were collected using a Hitachi H-7650 transmission electron microscope with 100 kV acceleration voltage. HRTEM, HAADF-STEM images and EDX mappings were obtained using a probe spherical aberration corrected JEM-ARM200F microscope with 200 kV accelerating voltage. SEM images were collected on a Nova NanoSEM 450 scanning electron microscope. XRD patterns were collected on the X-ray diffractometer (SmartLab SE, Rigaku) with Cu-Kα radiation (λ=0.1541 nm). ICP-OES (Avio 200, PerkinElmer) was used to determine the content of Ni. The GSB 04-1740-2004 Ni standard solution (1000 mg/L, Guobiao (Beijing) Testing & Certification Co., Ltd.) was used for ICP-OES. XPS spectra were obtained using an X-ray photoelectron spectrometer (K-alpha, Thermo Scientific) with a monochromatic Al Kα X-ray source (hυ=1486.6 eV). AFM images were collected on a scanning probe microscope (SPM-9700, Shimadzu). Zeta potentials were recorded on a Malvern Zetasizer Nano ZS 90 equipment.

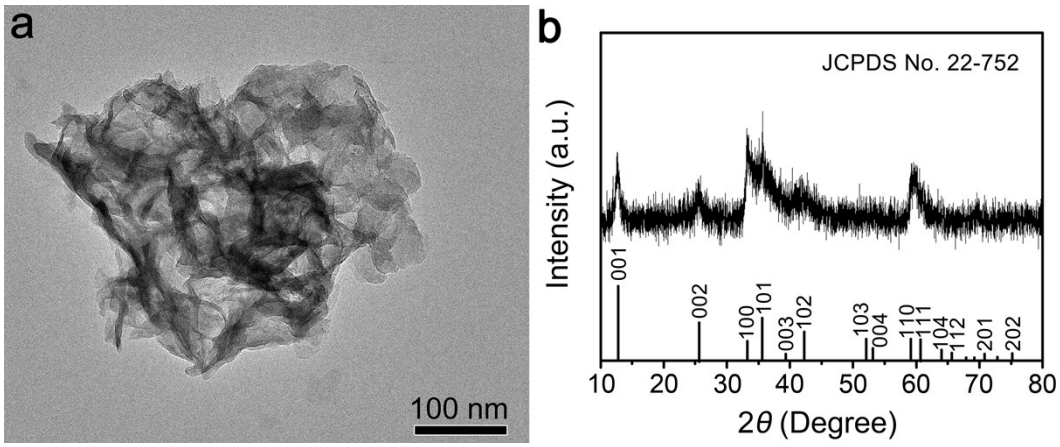

Fig. S1 (a) TEM image of $Ni(OH)_2$ nanosheets. (b) XRD pattern of $Ni(OH)_2$ nanosheets. The standard XRD profile for $Ni(OH)_2$ phase (JCPDS No. 22-752) is shown at the bottom.

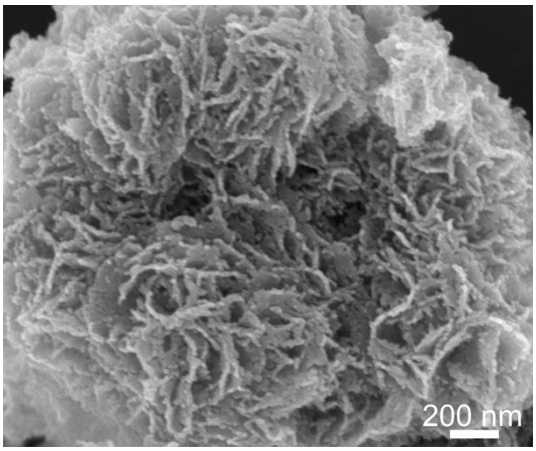

Fig. S2 SEM image of 4.3%N-Ni nanosheets.

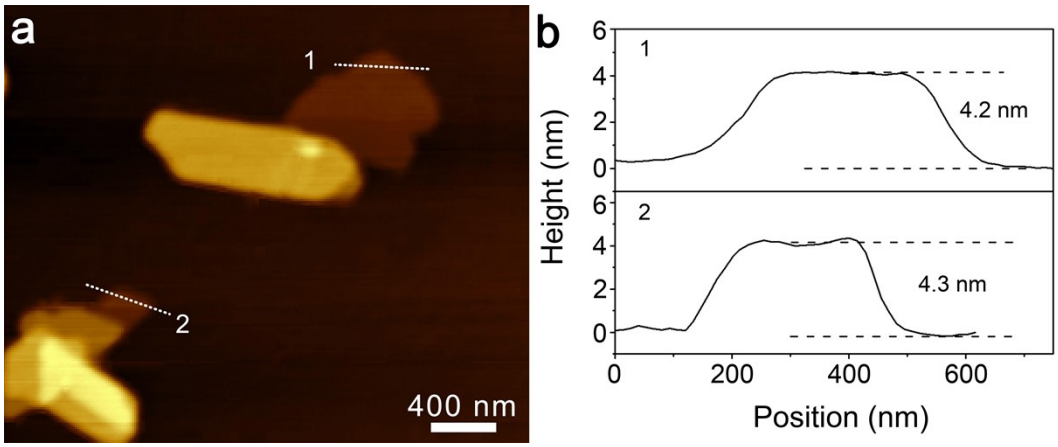

Fig. S3 (a) AFM image of 4.3%N-Ni nanosheets. (b) Height profiles along the direction marked in (a).

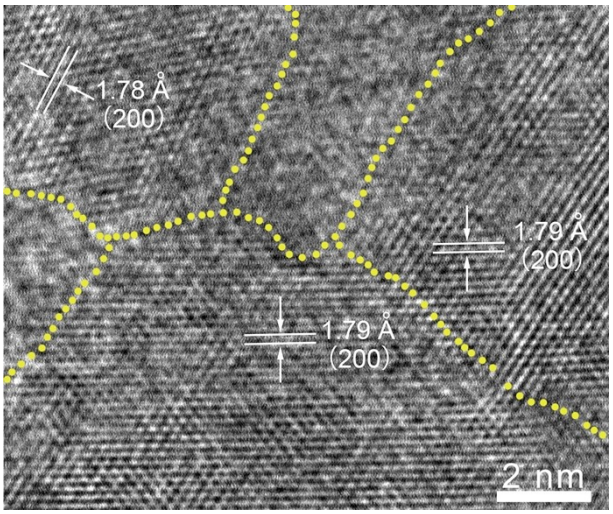

Fig. S4 HRTEM image of 4.3%N-Ni nanosheets.

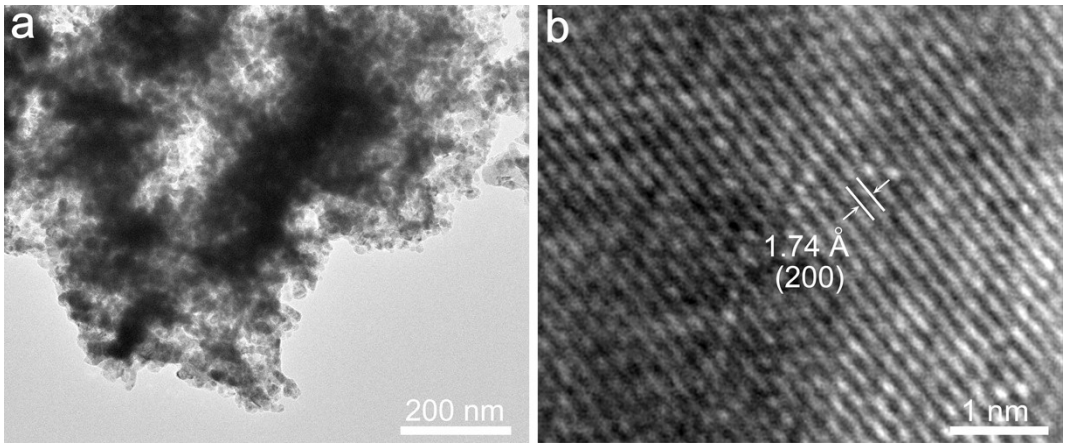

Fig. S5 (a) TEM image and (b) HRTEM image of pure Ni nanosheets.

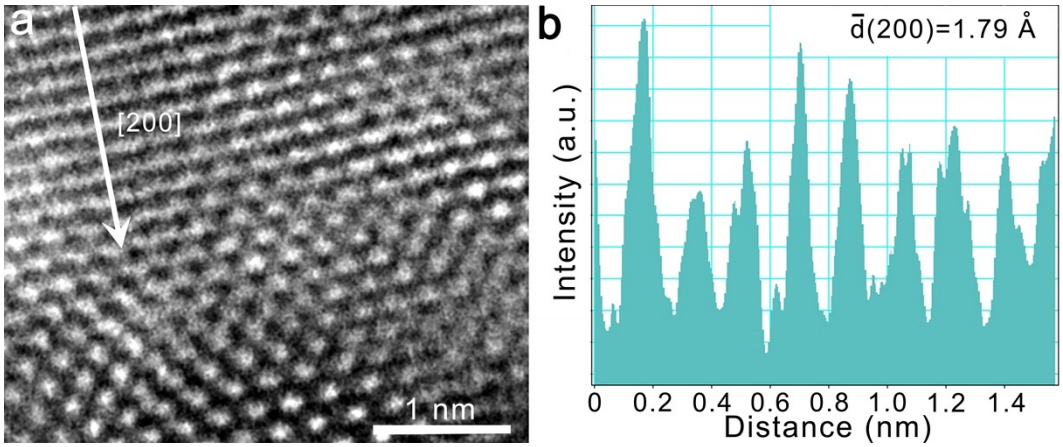

Fig. S6 (a) AC HAADF-STEM image of 4.3%N-Ni nanosheets. (b) Intensity profile recorded along the white line marked in (a).

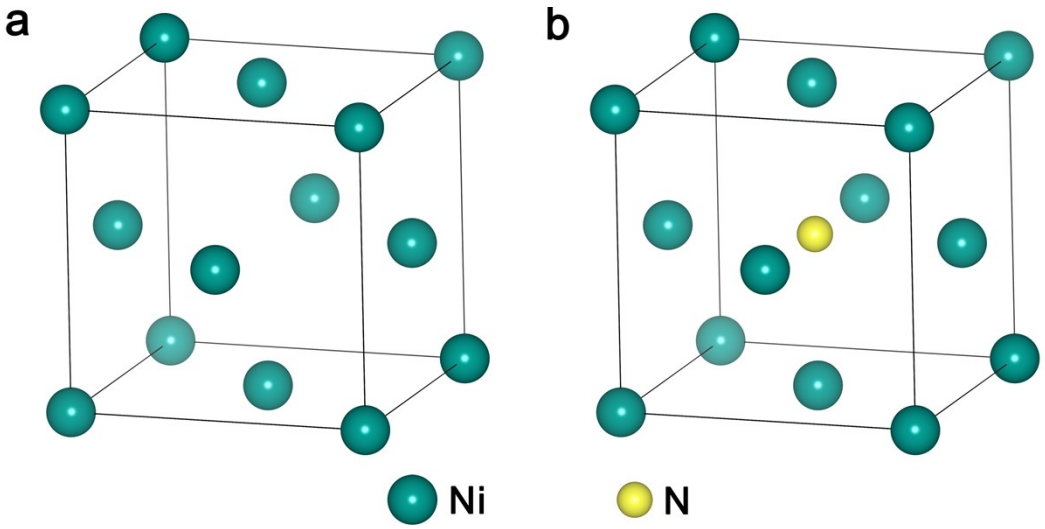

Fig. S7 Illustration of (a) Ni unit cell and (b) N-inserted Ni unit cell.

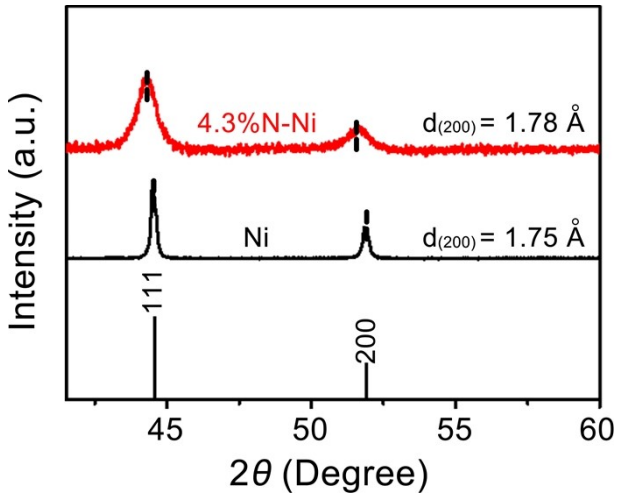

Fig. S8 Enlarged XRD patterns of pure Ni and 4.3%N-Ni nanosheets.

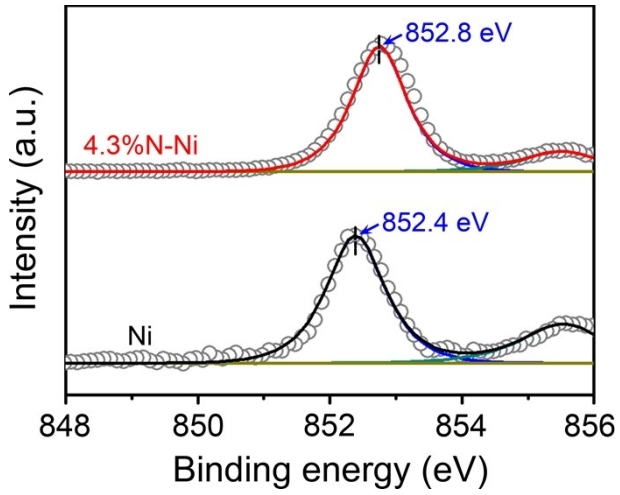

Fig. S9 Enlarged XPS spectra of pure Ni and 4.3%N-Ni nanosheets.

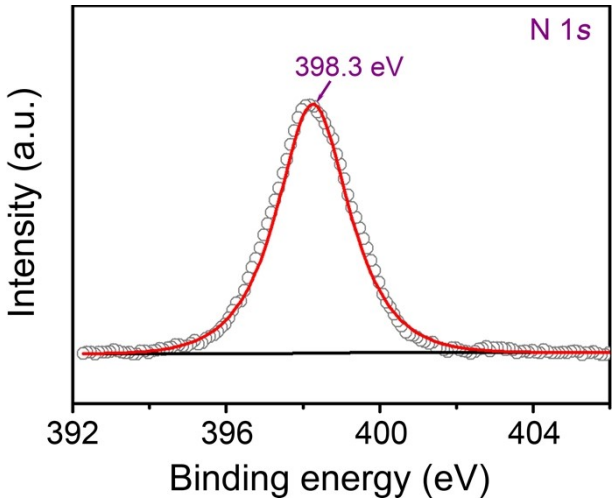

Fig. S10 N 1s XPS spectrum of 4.3%N-Ni nanosheets.

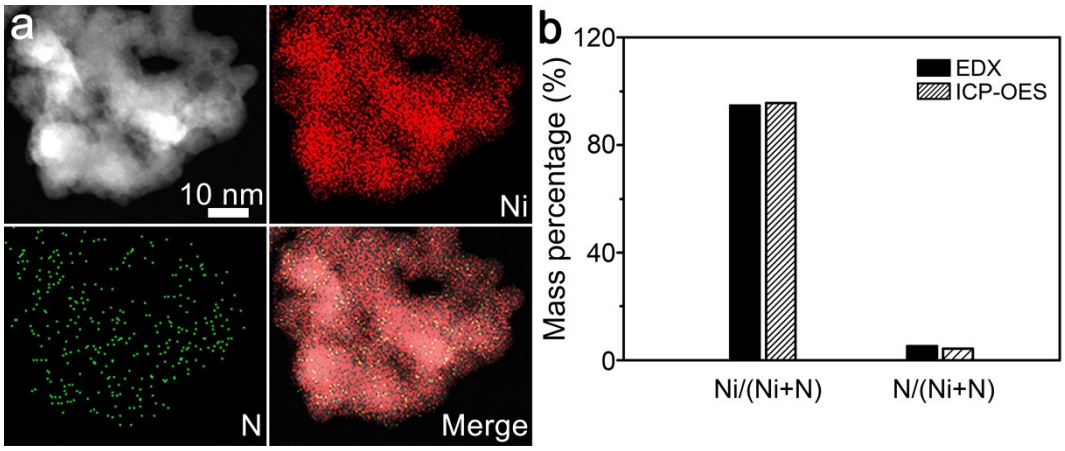

Fig. S11 (a) High-magnification STEM image and elemental mapping of Ni, N and merged image for an individual 4.3%N-Ni nanosheet. (b) Comparison of the content of Ni and N obtained by EDX and ICP-OES measurements.

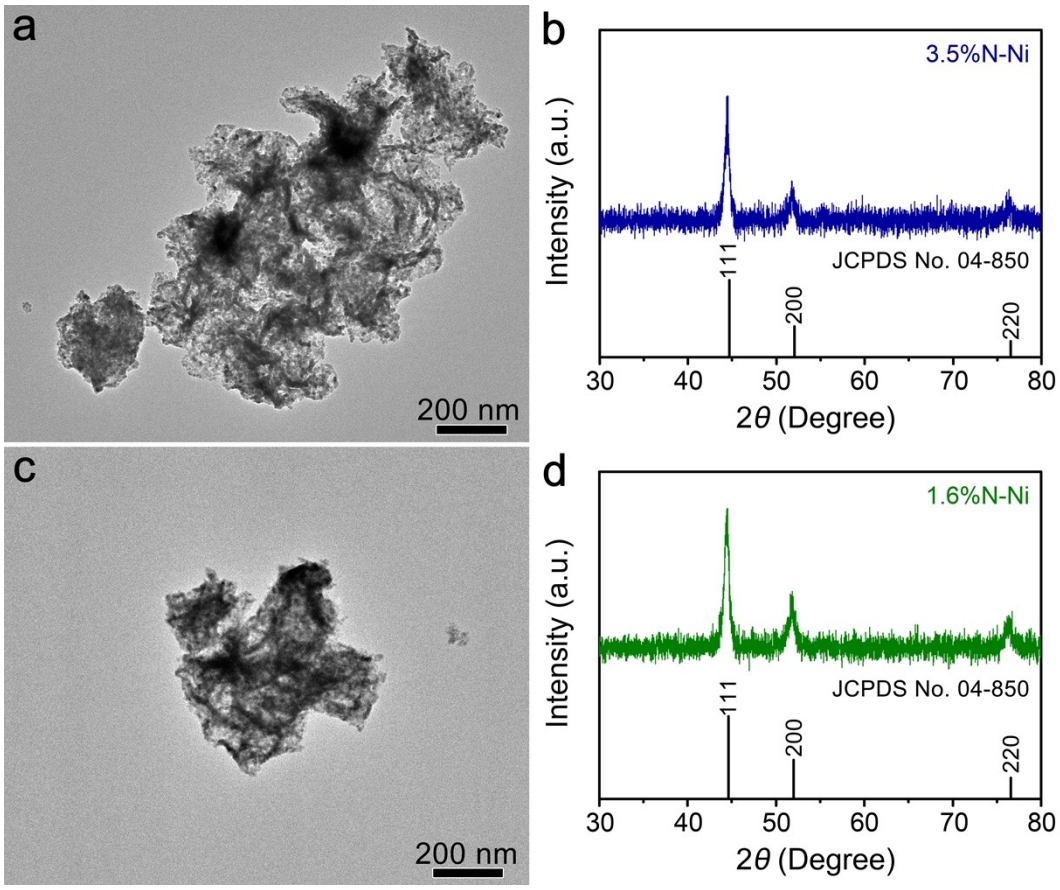

Fig. S12 (a, b) TEM image and XRD pattern of 3.5%N-Ni nanosheets. (c, d) TEM image and XRD pattern of 1.6%N-Ni nanosheets. The standard XRD patterns for fcc Ni (JCPDS No. 04-850) are attached at the bottom.

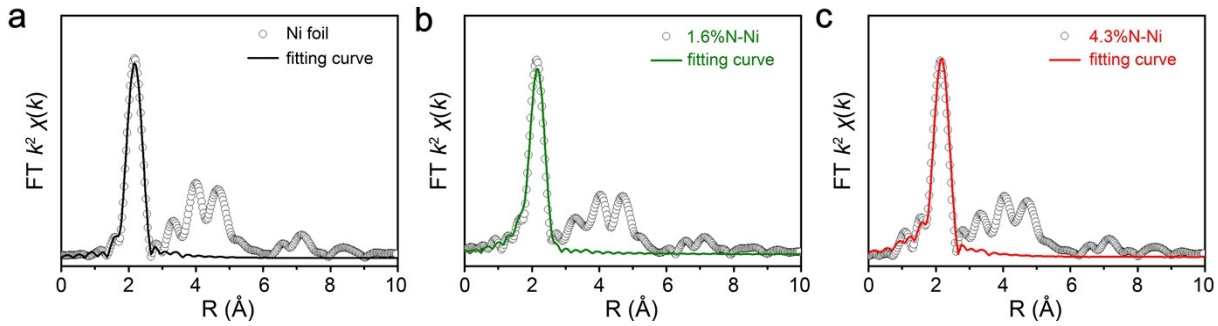

Fig. S13 EXAFS fitting curves for (a) Ni foil, (b) 1.6%N-Ni nanosheets, and (c) 4.3%N-Ni nanosheets.

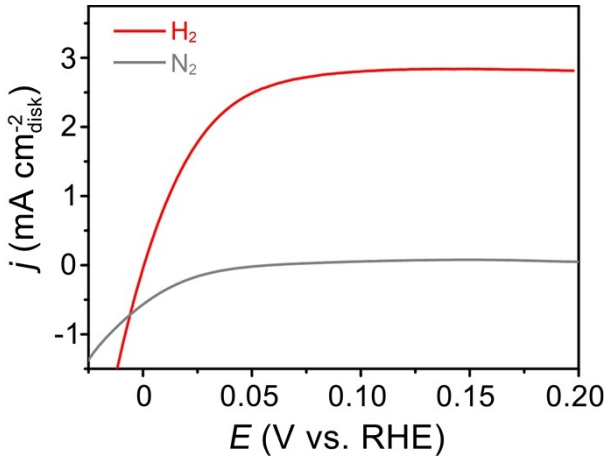

Fig. S14 Comparison of polarization curves of 4.3%N-Ni nanosheets recorded in H_2-saturated 0.1 M KOH and Ar-saturated 0.1 M KOH.

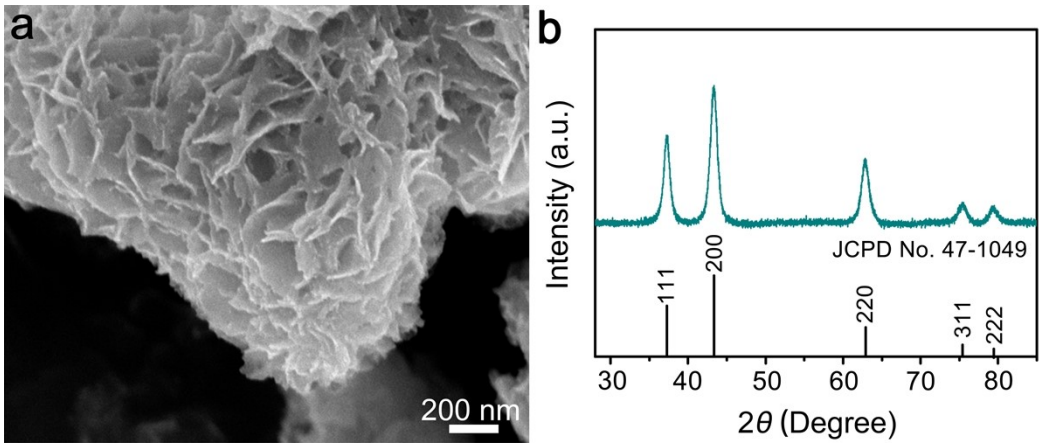

Fig. S15 (a) SEM image and (b) XRD pattern of NiO nanosheets. The NiO nanosheets were synthesized via the similar procedure with N-Ni nanosheets except using the air atmosphere.

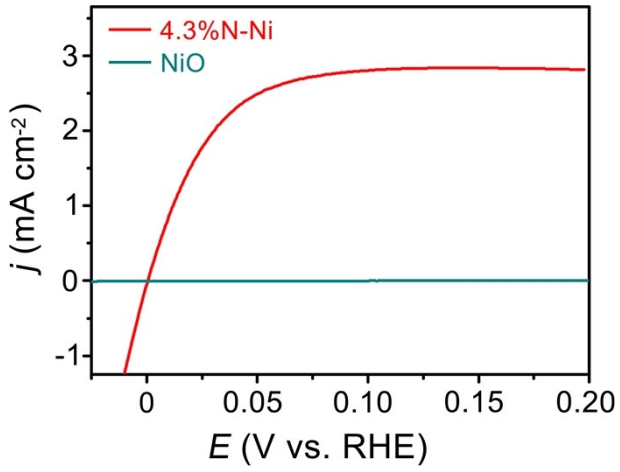

Fig. S16 HOR polarization curve of 4.3%N-Ni and NiO nanosheets.

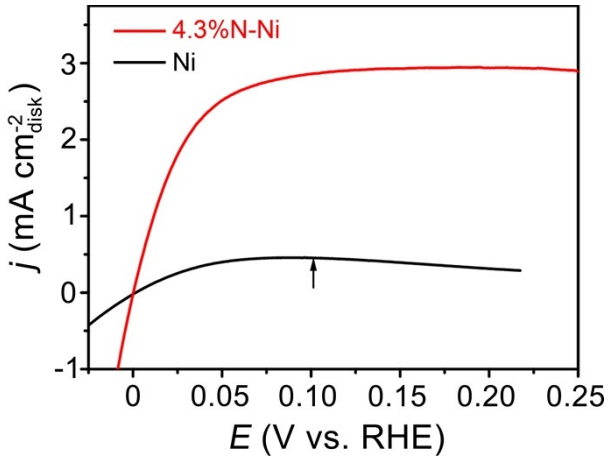

Fig. S17 Comparison of HOR polarization curves of 4.3%N-Ni and pure Ni nanosheets in the enlarged potential range.

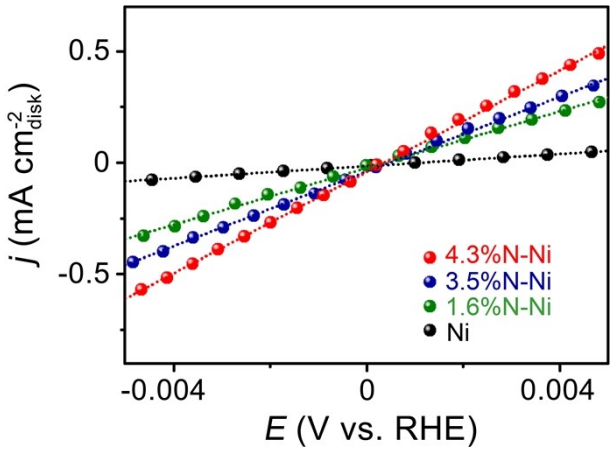

Fig. S18 Micro-polarization regions of 4.3%N-Ni, 3.5%N-Ni, 1.6%N-Ni, and pure Ni nanosheets.

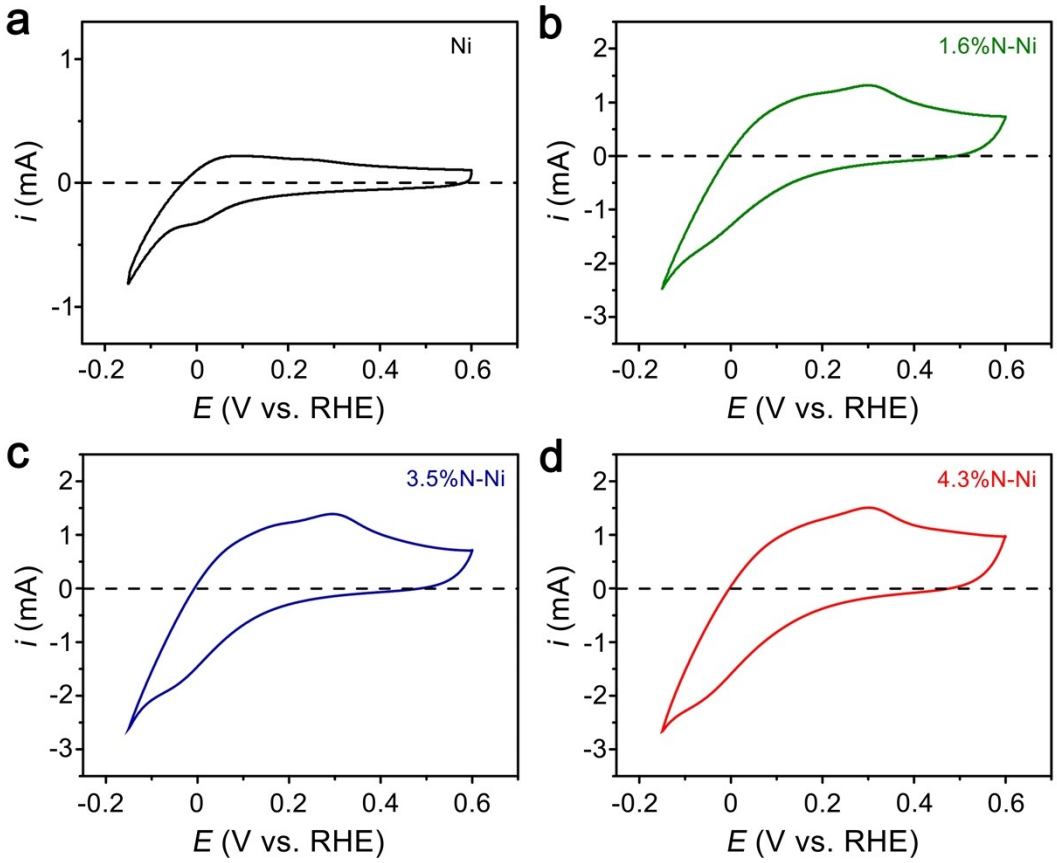

Fig. S19 Cyclic voltammetry of (a) Ni, (b) 1.6%N-Ni, (c) 3.5%N-Ni, and (d) 4.3%N-Ni nanosheets recorded in N_2-saturated 0.1 M KOH electrolyte with a sweep rate of 50 mV s^{-1}. ECSA could be evaluated from the OH desorption regions.

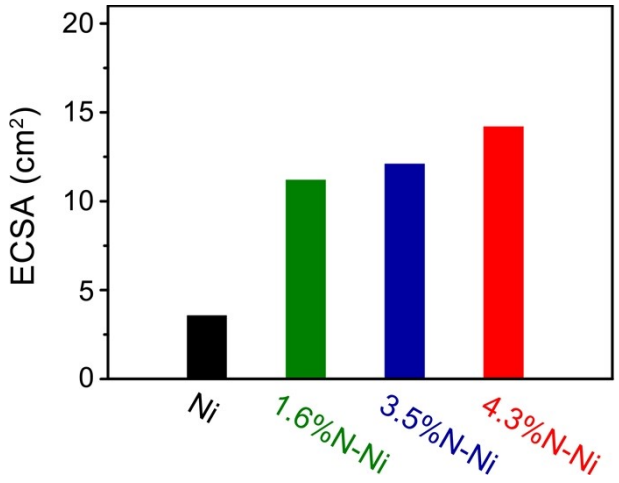

Fig. S20 Comparison of ECSAs for Ni and N-Ni nanosheets.

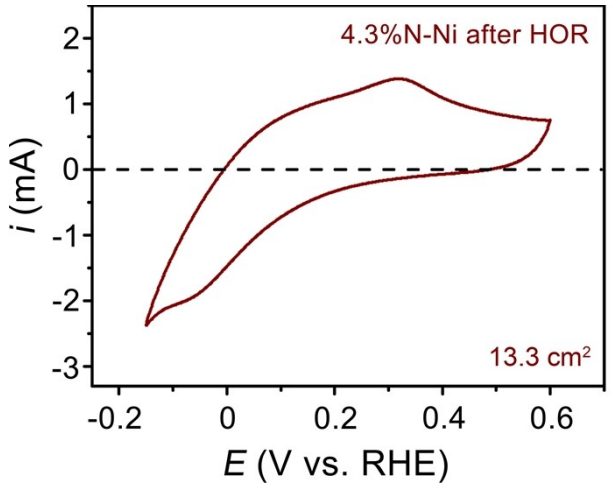

Fig. S21 Cyclic voltammetry of 4.3%N-Ni nanosheets after the long-term durability test. Inset shows the calculated ECSA value.

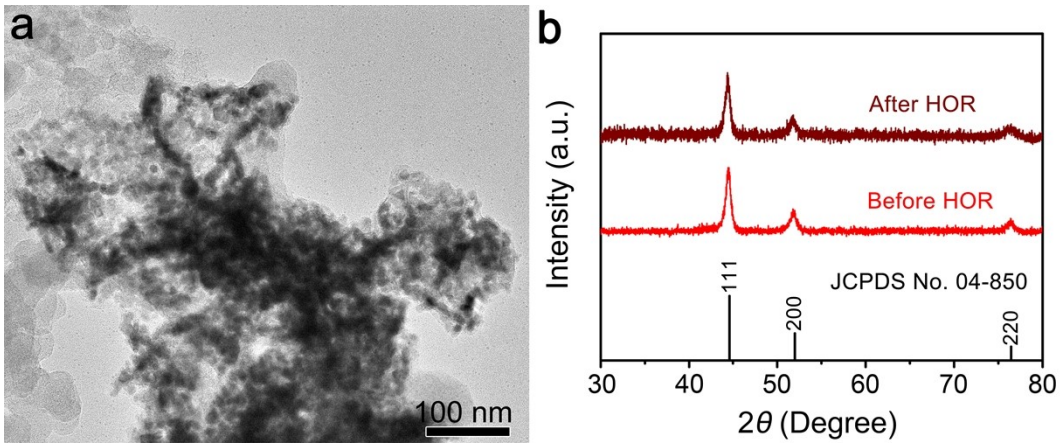

Fig. S22 (a) TEM image of 4.3%N-Ni nanosheets after the long-term durability test. (b) Comparison of XRD patterns of 4.3%N-Ni nanosheets before and after the durability test. The standard XRD profile for fcc Ni (JCPDS No. 04-850) is listed at the bottom.

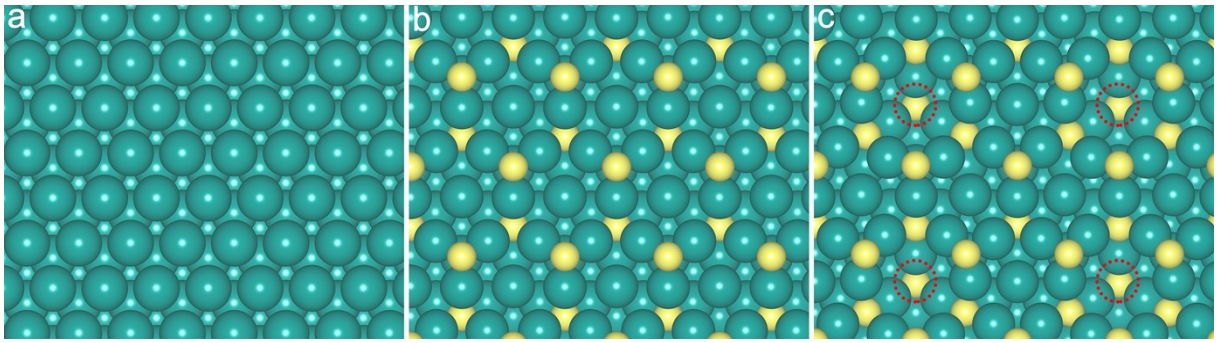

Fig. S23 Models of (a) pure Ni with (111) surface, (b) N-$Ni_{(f)}$ with flat (111) surface, and (c) N-$Ni_{(d)}$ with (111) surface containing Ni deficiencies. Cyan and yellow spheres represent Ni and N atoms, respectively. Red circles represent Ni deficiencies.

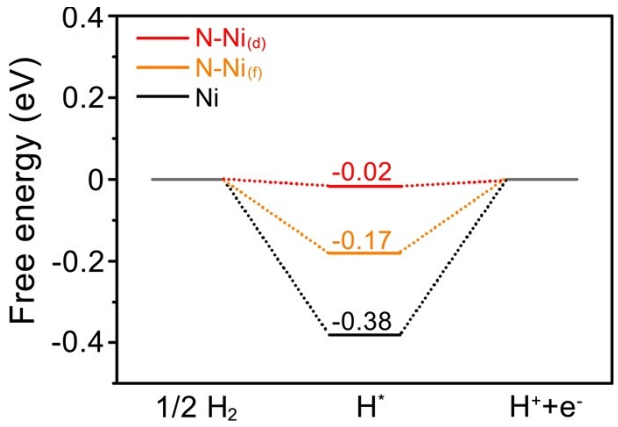

Fig. S24 Gibbs free energy for hydrogen adsorption on Ni, N-$Ni_{(f)}$ and N-$Ni_{(d)}$ structures.

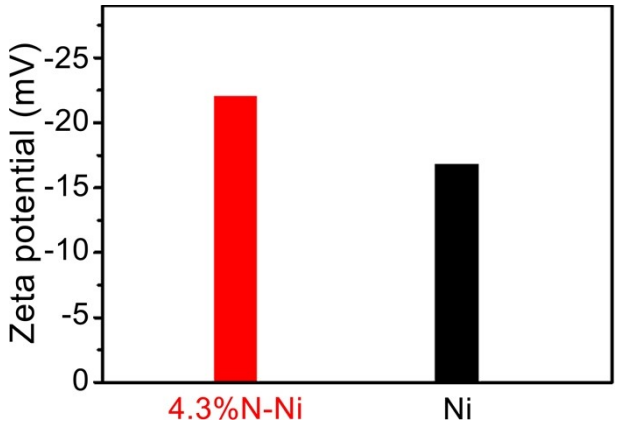

Fig. S25 Comparison of zeta potentials for 4.3%N-Ni and Ni.

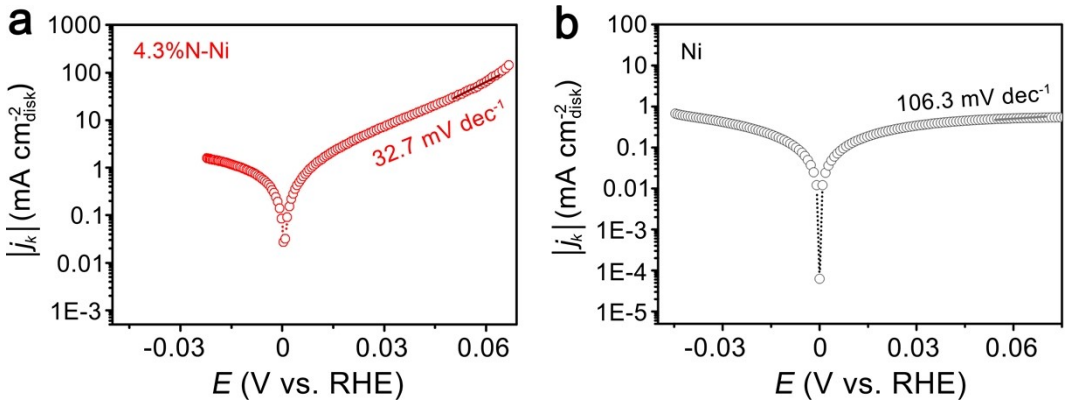

Fig. S26 Tafel plots of the kinetic current density on (a) 4.3%N-Ni and (b) pure Ni nanosheets in H_2-saturated 0.1 M KOH.

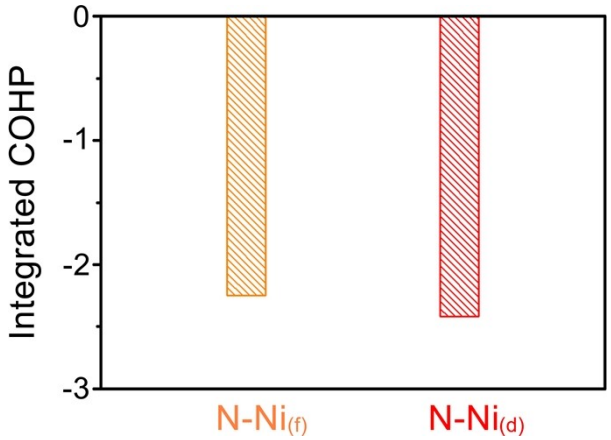

Fig. S27 Integrated COHP values from bonding/antibonding orbitals of N-$Ni_{(f)}$ and N-$Ni_{(d)}$ structures.

Table S1 XPS binding energies (eV) of the Ni 2*p* peaks for pure Ni and 4.3%N-Ni nanosheets.

Materials	Ni $2p_{3/2}$		Ni $2p_{1/2}$	
	Main peak	**Impurity peak**	**Main peak**	**Impurity peak**
Ni	852.4	855.5	869.8	873.3
4.3%N-Ni	852.8	855.5	870.2	873.3

Table S2 EXAFS fitting parameters at the Ni K-edge for tested samples.

Sample	Path	*CN*[(a)]	*R*(Å)[(b)]	σ^2 (Å^2)
Ni foil	Ni-Ni	10.44	2.480	0.00751
1.6%N-Ni	Ni-Ni	4.14	2.485	0.00899
	Ni-N	1.22	1.912	0.01630
4.3%N-Ni	Ni-Ni	3.108	2.490	0.00678
	Ni-N	1.702	1.911	0.02690

[(a)]*CN*, coordination number; [(b)]*R*, bond distance.

Table S3 HOR activity of reported non-noble metal-based catalysts in alkaline electrolyte.

Materials	Electrolyte	Rotating Speed (rpm)	Loading (mg cm^{-2})	$j_{k,m}$ @50 mV (mA mg$_{cat}^{-1}$)	$j_{0,s}$ (μA cm^{-2})	Reference
4.3%N-Ni nanosheet	0.1M KOH	1600	0.32	77.13	41	This work
Ni/N-CNTs	0.1M KOH	2500	0.25	9.3	28	S6
Ni-H_2	0.1M KOH	2500	0.14	50.4	28	S7
Ni/NiO	0.1M KOH	1600	0.5	5.0	26	S8
NiMo	0.1M NaOH	1600	0.1	/	27	S9
NiB/Ni	0.1M KOH	2500	0.142	24.7	26	S10
CoNiMo	0.1M KOH	1600	/	/	15	S11
Ni_3N	0.1M KOH	2500	0.31	24.38	14	S12
np-Ni_3N	0.1M KOH	1600	0.16	29.8	/	S13
Ni_3N/Ni/NF	0.1M KOH	/	/	/	3	S14
Ni/SC	0.1M KOH	2500	0.30	11.0	40.2	S15
NiCu	0.1M KOH	1600	/	/	25	S16
CeO_2/Ni	0.1M KOH	2500	0.306	12.28	38	S17
$Ni_{5.2}WCu_{2.2}$	0.1M KOH	/	/	2.55	14	S18

Table S4 Summary of the exchange current density calculated from micro-polarization regions and Tafel regions.

Materials	Exchange current density (mA cm^{-2})	
	Micro-polarization regions	Tafel regions
Pure Ni nanosheet	0.36	0.36
1.6%N-Ni nanosheet	1.66	1.66
3.5%N-Ni nanosheet	2.19	2.15
4.3%N-Ni nanosheet	2.96	2.94

References

1 H. C. Chen, Y. L. Qin, H. J. Cao, X. X. Song, C. H. Huang, H. B. Feng, X. S. Zhao, *Energy Storage Mater.* 2019, **17**, 194-203.

2 J. P. Perdew, K. Burke, M. Ernzerhof, *Phys. Rev. Lett.* 1996, **77**, 3865.

3 G. Kresse, D. Joubert, *Phys. Rev. B* 1999, **59**, 1758.

4 S. Grimme, *J. Comput. Chem.* 2006, **27**, 1787-1799.

5 M. Liu, Y. J. Peng, B. Zhang, P. D. Luna, O. Voznyy, J. X. Xu, X. L. Zheng, C. T. Dinh, F. J. Fan, C. H. Cao, F. P. G. de Arquer, T. S. Safaei, A. Mepham, A. Klinkova, E. Kumacheva, T. Filleter, D. Sinton, S. O. Kelley, E. H. Sargent, *Nature* 2016, **537**, 382-386.

6 Z. B. Zhuang, S. A. Giles, J. Zheng, G. R. Jenness, S. Caratzoulas, D. G. Vlachos, Y. S. Yan, *Nat. Commun.* 2016, **7**, 10141.

7 W. Y. Ni, T. Wang, P. A. Schouwink, Y. C. Chuang, H. M. Chen, X. L. Hu, *Angew. Chem. Int. Ed.* 2020, **59**, 10797-10801.

8 Y. Yang, X. D. Sun, G. Q. Han, X. Liu, X. Y. Zhang, Y. F. Sun, M. Zhang, Z. Cao, Y. J. Sun, *Angew. Chem. Int. Ed.* 2019, **58**, 10644-10649.

9 S. Kabir, K. Lemire, K. Artyushkova, A. Roy, M. Odgaard, D. Schlueter, A. Oshchepkov, A. Bonnefont, E. Savinova, D. C. Sabarirajan, P. Mandal, E. J. Crumlin, I. V. Zenyuk, P. Atanassov, A. Serov, *J. Mater. Chem. A* 2017, **5**, 24433-24443.

10 F. L. Yang, P. Y. Han, N. Yao, G. Z. Cheng, S. L. Chen, W. Luo, *Chem. Sci.* 2020, **11**, 12118-12123.

11 W. C. Sheng, A. P. Bivens, M. Myint, Z. B. Zhuang, R. V. Forest, Q. R. Fang, J. G. Chen, Y. S. Yan, *Energy Environ. Sci.* 2014, **7**, 1719-1724.

12 W. Y. Ni, A. Krammer, C. S. Hsu, H. M. Chen, A. Schuler, X. L. Hu, *Angew. Chem. Int. Ed.* 2019, **58**, 7445-*7449*.

13 T. T. Wang, M. Wang, H. Yang, M. Q. Xu, C. D. Zuo, K. Feng, M. Xie, J. Deng, J. Zhong, W. Zhou, T. Cheng, Y. G. Li, *Energy Environ. Sci.* 2019, **12**, 3522-3529.

14 F. Z. Song, W. Li, J. Q. Yang, G. Q. Han, P. L. Liao, Y. J. Sun, *Nat. Commun.* 2018, **9**, 4531.

15 F. L. Yang, X. Biao, Y. M. Zhao, X. W. Wang, G. Z. Cheng, W. Luo, *J. Mater. Chem. A* 2019, **7**,

10936-10941.

16 A. Roy, M. R. Talarposhti, S. J. Normile, I. V. Zenyuk, V. D. Andrade, K. Artyushkova, A. Serov, P. Atanassov, *Sustain. Energy Fuels* 2018, **2**, 2268-2275.

17 F. L. Yang, X. Bao, P. Li, X. W. Wang, G. Z. Cheng, S. L. Chen, W. Luo, *Angew. Chem. Int. Ed.* 2019, **58**, 14179-14183.

18 S. Qin, Y. Duan, X. L. Zhang, L. R. Zheng, F. Y. Gao, P. P. Yang, Z. Z. Niu, R. Liu, Y. Yang, X. S. Zheng, J. F. Zhu, M. R. Gao, *Nat. Commun.* 2021, **12**, 2686.